JOURNAL OF SOLID STATE CHEMISTRY 54, 346–357 (1984)

The Nonmetal–Metal Transition and Phase Separation in the Europium–Ammonia System*,†

P. S. HSU, C. B. ZIMM‡, AND W. S. GLAUNSINGER§

Department of Chemistry, Arizona State University, Tempe, Arizona 85287

Received April 23, 1984

The coexistence curve of Eu–NH_3 solutions has been determined by visual observation and electron paramagnetic resonance (EPR). A nonmetal–metal transition is evident in Eu–NH_3 solutions, and the miscibility gap is the most pronounced among the metal–ammonia (M–NH_3) systems that have been studied. The critical concentration and temperature are 1.30 mole% metal and 321 K, respectively. The coexistence curve has a parabolic shape within close vicinity of the critical point, which strongly suggests the existence of long-range interactions and cluster formation. EPR spectra indicate that the cation–electron interactions in these solutions are weak, so that the valence-electron concentration in M–NH_3 solutions is probably the primary factor in determining the nature of the nonmetal–metal transition. The coexistence curve and associated critical parameters for Eu–NH_3 solutions are compared to those obtained for other M–NH_3 solutions.

Introduction

Metal–ammonia (M–NH_3) solutions exhibit a rich variety of physical behavior as the metallic concentration is varied, and during the past century they have served as most useful model systems for developing and testing concepts in solution chemistry (*1–5*). In very dilute solutions the metal is ionized, with the valence electron(s) of the metal surrounded by solvent molecules. The solvated electron has an extremely long lifetime in M-NH_3 solutions and has been the subject of numerous investigations. As the metallic concentration is increased, electron–ion interactions become important and a variety of associated species can be formed involving M^+ and e^-, such as M, M^-, M_2, and e_2^{2-}, where M is either an ion pair or an expanded-metal monomer, M^- is a diamagnetic anion resulting from the addition of an electron to the ion pair or monomer, M_2 is a diamagnetic dimer formed from the union of two ion pairs or monomers, and e_2^{2-} is a diamagnetic dielectron species consisting of two electrons in close proximity. At intermediate concentrations the electronic wavefunctions overlap sufficiently to cause a nonmetal–metal transition, which is dramatically illustrated by the miscibility gap in the phase diagrams of many M–NH_3 solutions. One advantage of these solutions over solids for detailed studies of this transitional region is that they are not plagued

* We would like to dedicate this paper to the memory of Professor M. J. Sienko.

† This research was sponsored by National Science Foundation Grant DMR 82-15315.

‡ Present address: Los Alamos National Laboratory, Los Alamos, New Mexico 87544.

§ To whom correspondence should be addressed.

0022-4596/84 $3.00

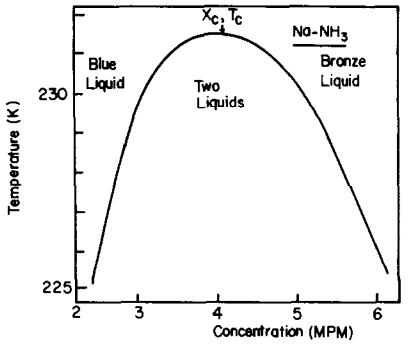

FIG. 1. Coexistence curve for Na–NH_3 solutions (*8*). Abscissa in mole% metal (MPM).

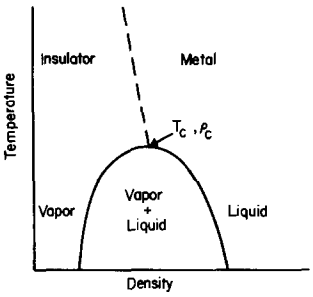

FIG. 2. Schematic phase diagram for dense metal vapors exhibiting an insulator–metal transition (*9*).

by abrupt structural transformations (*6*). Finally, in the concentrated region *M*–NH_3 solutions behave as relatively simple liquid metals, although the *M*–NH_3 compounds that can be formed by freezing concentrated solutions exhibit some of the most unusual and remarkable properties of any solids (*7*).

One of the most striking properties of many M–NH_3 solutions is the immiscibility of dilute and concentrated solutions over a wide range of temperatures and compositions. The Na–NH_3 coexistence curve, which has been very carefully measured by Chieux and Sienko (*8*) and is depicted in Fig. 1, is typical of the phase behavior of these solutions in the region of the nonmetal–metal transition. Above the critical temperature T_c, Na–NH_3 solutions are homogeneous. However, below T_c within the miscibility gap, these solutions separate into two distinct phases: a more dilute, blue, nonmetallic liquid and a more concentrated, bronze, metallic solution. As pointed out by Chieux and Sienko (*8*), such a coexistence curve bears a very close resemblance to that postulated by Krumhansl (*9*) for dense metal vapors shown in Fig. 2. He argues that phase separation may well accompany the insulator–metal transition due to the much different electronic free energies of these two electronic phases.

Taking free energies appropriate to a van der Waals fluid at large atomic volumes (insulating phase) and to a Wigner–Seitz metal at small atomic volumes (metallic phase), the general variation of the free energy with atomic volume both below and above T_c is schematically represented in Fig. 3. For $T < T_c$, a first-order phase transition is expected at atomic volumes corresponding to the two points of common tangency. For $T \geq T_c$, the two points converge, and the two electronic phases become mixed. Historically, Pitzer (*10*) first recognized the above analogy between the nonmetal–metal transition in *M*–NH_3 solutions and vapor–liquid condensation below T_c. He proposed that NH_3 can be regarded as a dielectric medium in which the metal atoms undergo a vapor–liquid condensation below T_c, with the nonmetallic solutions corresponding to a gas of metal atoms and the metallic solutions to a pure liquid metal.

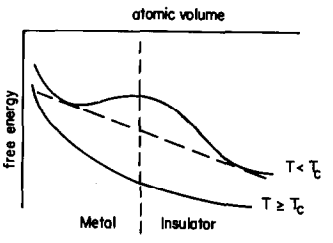

FIG. 3. Schematic variation of the free energy with atomic volume near the insulator–metal transition (*9*).

In spite of the close similarity between Figs. 1 and 2, there is not a one-to-one correspondence between the electronic properties of M–NH_3 solutions and the behavior predicted in Fig. 2. Although there is indeed a nonmetal–metal transition as the metallic concentration is increased in the one-liquid region above T_c, the transition is not abrupt, as originally proposed by Mott (*11*). Careful measurements of the shape of the coexistence curve near T_c by Chieux and Sienko (*8*) in Na–NH_3 solutions and Teoh *et al.* (*12*) in Ca–NH_3 solutions have indicated that it is parabolic for $(T_c - T)/T_c \gtrsim 10^{-2}$, which is in agreement with the predictions of both simple molecular-field and van der Waals theories. Widom (*13*) has considered the coexistence curve for a fluid near its liquid–vapor critical point and found that for parabolic curves the intermolecular forces extend to infinity. Such considerations led Sienko (*14*) to suggest that the origin of the parabolic coexistence curve in M–NH_3 solutions may involve long-range interactions and cluster formation. Although there have been no reports of the direct observation of clusters in M–NH_3 solutions, the formation of clusters or microprecipitates in imperfect solids is a ubiquitous phenomenon. In fact, one anticipates the formation of dynamic clusters in these solutions as a result of density fluctuations, where fluctuations to lower density tend to localize electrons and fluctuations to higher density are conducive to electronic delocalization. If such clusters indeed occur near the nonmetal–metal transition in M–NH_3 solutions above T_c, then the transition would not be expected to be abrupt due to the statistical distribution of cluster sizes. In this case, the observed phase separation within the miscibility gap may represent a macroscopic manifestation of the coexistence of nonmetallic and metallic clusters in M–NH_3 solutions.

Several, but not all, M–NH_3 solutions exhibit phase separation (*15*). A miscibility gap exists in Li– (*16*), Na– (*8*), K– (*16*), and Ca–NH_3 (*12*) solutions, but not in Rb (*17*) and Cs–NH_3 (*18*) solutions. Empirically, phase separation seems to occur when the radius of the cation ($r_{M^{z+}}$) is substantially less ($\lesssim$0.1 Å) than the radius of NH_3 ($\simeq$1.5 Å). On this basis, Eu–NH_3 ($r_{Eu^{2+}}$ = 1.12 Å) solutions as well as the other divalent M–NH_3 solutions should show phase separation, but to date they have not been studied in any detail.

In this paper we present and discuss the results of our determination of the coexistence curve of Eu–NH_3 solutions and associated critical parameters and compare these results to those obtained for other M–NH_3 solutions.

Experimental

Anhydrous ammonia, purchased from Matheson, was 99.99% pure. High-purity natural Eu was supplied by Ames Laboratory at Iowa State University, and enriched Eu (^{153}Eu—98.8%) was obtained from Oak Ridge National Laboratory. All samples were prepared on a high-vacuum line by reacting Eu with NH_3 in a specially cleaned 3-mm-i.d. quartz electron paramagnetic resonance (EPR) tube. The tubes were sealed carefully because they had to withstand the relatively high interval pressures ($\simeq$40 atm) when the samples were heated to temperatures as high as 350 K. The solution concentration was varied between 10^{-4} and 14.3 mole% metal (MPM).

Although a variety of techniques have been employed to identify phase boundaries in M–NH_3 solutions, with the most common ones being visual observation (*16*), vapor-pressure determinations (*19*), and electrical-conductivity measurements (*20*), they all have their individual drawbacks. With the visual method, it is oftentimes difficult to differentiate the two phases near the phase boundary, particularly at higher temperatures where decom-

position is more pronounced. Vapor-pressure measurements are plagued by the hydrogen evolution accompanying decomposition. Most quantitative studies of the phase diagrams of M–NH_3 solution have involved measurements of the temperature dependence of the electrical conductivity, but even here variations in the distribution of the two phases as well as the conductivity temperature coefficient within a given phase have caused difficulties.

We have used direct visual observation as the primary method for determining the phase boundaries in Eu–NH_3 solutions. We resorted to this technique because of the instability of these solutions and the high temperatures required to map out the miscibility gap (T_c = 321 K), which frequently necessitated a relatively rapid determination of the phase boundary. For temperatures below ambient, a dry-ice ethanol bath (195 K) was prepared in a 4-liter Dewar containing a heater to increase the temperature, and a magnetic stirrer to ensure temperature homogeneity. For temperatures above ambient, a stirred oil bath was employed, and the temperature was regulated with a hot plate. In general, the sample was shaken, immersed in a constant-temperature bath stable to within 0.1 K, and then withdrawn from the bath briefly to determine if either one or two phases were present. If two phases were observed, then the temperature was raised in 10 K increments until only one phase was present. Then the temperature was decreased very slowly until the second phase just reappeared, which corresponds to a point on the temperature vs composition phase diagram. For a given composition, the temperature of the phase separation was the same both on heating and cooling cycles. Below ambient temperature, duplicate and triplicate determinations on the same sample were in good agreement. However, above ambient temperature, the solutions were sufficiently unstable that repeated experiments on the same sample were usually difficult, so that normally three independent preparations of the same sample were used to evaluate the reproducibility of the phase separation. The phase separation was reproducible to better than 2 K, and the data reported in this paper represent the average values for three successful independent determinations.

EPR has been used as a secondary technique for phase-boundary determinations. A Bruker-IBM ER 200-D spectrometer operating at X-band in the range 100–700 K was used for these experiments. The modulation frequency was 100 kHz, and the microwave power was reduced sufficiently to avoid saturation. The sample height was about 1 cm, so that the entire sample could be placed in the TE_{102} EPR resonator. The temperature gradient along the vertical dimension of the sample was less than 1 K.

Results

Several samples having a Eu concentration above about 0.5 MPM were surprisingly stable in that they could be heated to temperatures as high as 350 K without significant decomposition. Moreover, in contrast to other M–NH_3 solutions (except Yb–NH_3 solutions (*21*)), Eu–NH_3 solutions separate into a blue insulating phase that floats on top of the bronze metallic phase.

The coexistence curve for Eu–NH_3 solutions determined from both visual observations and EPR is shown in Fig. 4. For comparison, the corresponding coexistence curves for the alkali M–NH_3 solutions (*16*) are also reproduced. It is apparent that the Eu–NH_3 curve has a very pronounced maximum, a much higher T_c, and a substantially lower x_c than the alkali M–NH_3 solutions.

The available data on the coexistence curves for Ca–NH_3 (*12*) and Yb–NH_3 (*21*) solutions are compared to the Eu–NH_3 curve in Fig. 5. Qualitatively, the Ca–NH_3 and Eu–NH_3 curves are similar, but T_c is higher and x_c lower for the latter system.

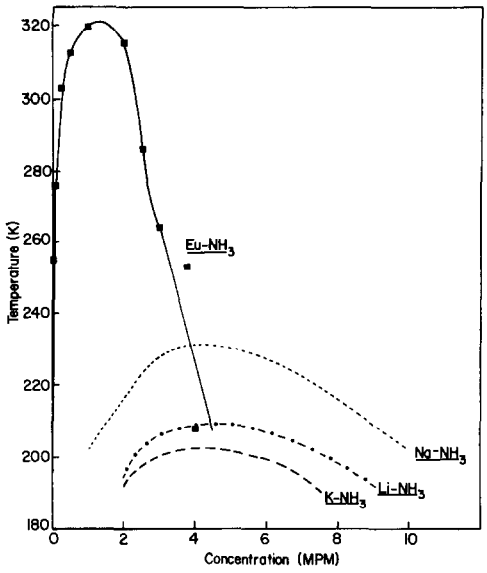

FIG. 4. Comparison of the coexistence curve for Eu–NH_3 solutions with those for the alkali metal–ammonia solutions (*16*).

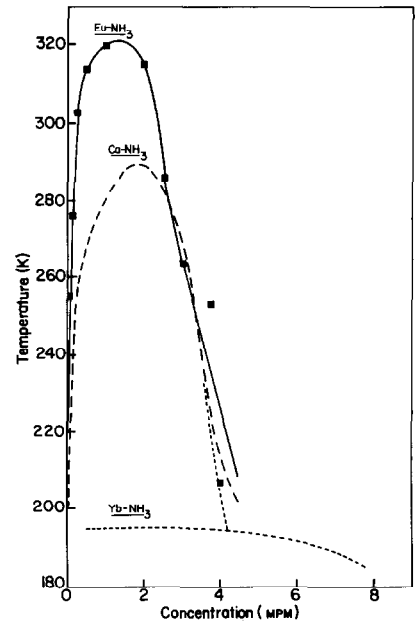

FIG. 5. Comparison of the coexistence curve for Eu–NH_3 solutions with those for Ca–NH_3 (*2*) and Yb–NH_3 (*21*) solutions.

The data for Yb–NH_3 solutions do not extend to low enough concentrations to define the miscibility gap. The critical concentrations and temperatures of M–NH_3 systems are summarized in Table I, where it is evident that x_c decreases and T_c increases in going from monovalent to divalent metals dissolved in NH_3.

TABLE I

CRITICAL POINTS OF METAL–AMMONIA SOLUTIONS

Solution	x_c (MPM)[a]	T_c (K)[a]
Li–NH_3	4.32	209.7
Na–NH_3	4.12	231.5
K–NH_3	4.35	203.2
Ca–NH_3	1.68	290.0
Eu–NH_3	1.30	321

[a] Values from Li–, Na–, K–, Ca–, and Eu–NH_3 solutions are from Refs. (*16*), (*14*), (*16*), (*12*), and this work, respectively.

The phase diagram of the Ca–NH_3 system (*22*) over a wide range of compositions is shown in Fig. 6. The maximum melting-point bump near 14 MPM is indicative of compound formation at the stoichiometry $Ca(NH_3)_6$, which has been confirmed in

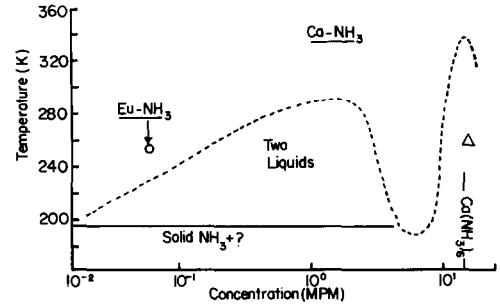

FIG. 6. Phase diagram of Ca–NH_3 solutions using a logarithmic concentration scale (*22*). The open triangle represents our measurement of the melting point of $Ca(NH_3)_6$, and the open circle is a point on the Eu–NH_3 phase diagram determined by EPR.

several solid-state studies (*7*). However, we have found that the $Ca(NH_3)_6$ compound melts near 260 K from visual observation, EPR, and previous resistivity (*23*) measurements. It is noteworthy that the two-liquid region of the Ca–NH_3 phase diagram extends to very low concentrations, so that care must be exercised to avoid phase separation even in dilute solutions. Dilute Eu–NH_3 solutions also separate at lower temperatures, but in these solutions the tendency is even more marked than in Ca–NH_3 solutions (see Figs. 5 and 6).

We have found EPR to be an extremely useful secondary technique to probe the phase diagram of Eu–NH_3 solutions. In these solutions there are two distinct paramagnetic species: Eu^{2+}, which has a spherically symmetric electronic configuration $4f^7 5s^2 5p^6$ in the ionic state $^8S_{7/2}$, and unpaired electrons, which become increasingly delocalized as the metallic concentration is increased. The nuclear magnetic moment of Eu (^{151}Eu = 47.8% abundant, I = 5/2; ^{153}Eu = 52.2% abundant, I = 5/2) provides another magnetic probe of these solutions via the hyperfine interaction. In a first-order approximation, a six-line hyperfine pattern is produced for each isotope, with the ratio of the hyperfine coupling constants, A, equal to that of their nuclear moments, i.e., $^{151}A/^{153}A = {}^{151}\mu/{}^{153}\mu = 2.269$. In samples containing natural Eu, ^{151}A can be determined from the separation of the low- and high-field peaks in the hyperfine pattern, and ^{153}A can then be calculated from the relation $^{153}A = {}^{151}A/2.269$ (*24*). Moreover, the possible presence of $Eu(NH_2)_2$ from sample decomposition poses no problem, because it is insoluble in these solutions (*25*) and has a characteristic EPR signal (*26*).

The EPR spectra in Eu–NH_3 solutions strongly depend on both concentration and temperature. The concentration dependence of the EPR spectra is illustrated in Figs. 7–9. In the most dilute solutions (10^{-4} MPM) the EPR spectrum consists of a single, narrow, symmetrical Lorentzian line having a peak-to-peak linewidth of about 2 G and a g-factor of 2.000. Both the EPR line and g-value strongly resemble those for dilute alkali M–NH_3 solutions (*25, 27*), where the spectrum has been attributed to solvated electrons. Since the integrated intensity of this line corresponds to about twice the Eu^{2+} concentration, and the line disappears upon sample decomposition, we also conclude that it must be due to solvated electrons. However, the linewidths are nearly an order of magnitude greater than those in dilute alkali M–NH_3 solutions. Therefore, magnetic interactions between solvated electrons and Eu^{2+} cations, which enhance the electronic relaxation rate and hence broaden the solvated-electron line, persist even at concentrations as low as 10^{-4} MPM.

As the concentration is increased within the dilute range, the solvated-electron line broadens due to the increasing magnetic Eu^{2+} reservoir to which the solvated electron relaxes, and the EPR spectrum of Eu^{2+} appears (Fig. 7). Only the Eu^{2+} spectrum can be observed above about 5×10^{-3} MPM, and in the dilute range the hyperfine interactions can be resolved (Figs. 6 and 7). The EPR spectrum shown in Fig. 7b can be fitted with ^{151}A = 36.7 G, ^{153}A = 16.2 G, and g = 1.996, which are characteristic of Eu^{2+} (*24*).

Although such dilute solutions show no evidence of phase separation, in more concentrated solutions phase separation is apparent in the Eu^{2+} EPR spectra (Fig. 8). At higher concentrations ($\gtrsim 2 \times 10^{-2}$ MPM) in the one-liquid region, only a single asymmetric line is observed, presumably because exchange interactions between the Eu^{2+} moments average out the hyperfine interaction, and because the electrical conductivity is sufficiently high to prevent the microwaves from penetrating the sample uniformly (skin effect) (*24*). Upon phase

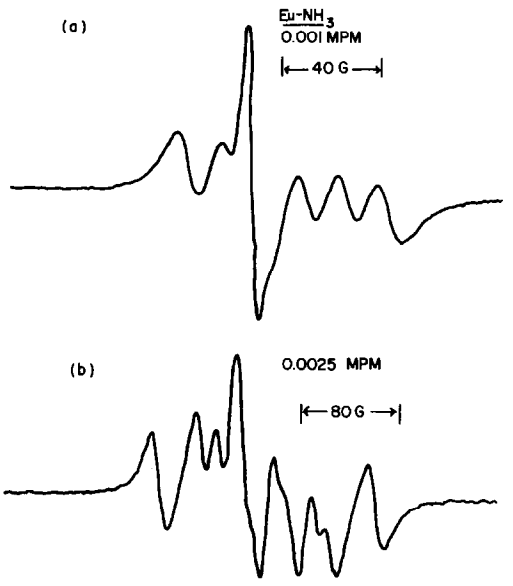

FIG. 7. Typical first-derivative EPR spectra for dilute Eu–NH_3 solutions containing enriched Eu (^{153}Eu—98.8%) (a) and natural Eu(b). The sample temperature and microwave frequency are 225 K and 9.40 GHz. The solvated-electron line as well as the six-line $^{153}Eu^{2+}$ hyperfine structure are resolved in spectrum (a), and in spectrum (b) primarily the Eu^{2+} hyperfine splitting is observed. There is no phase separation at these concentrations.

separation, there are two distinct phases in the microwave resonator, with each phase having its characteristic EPR spectrum. Since the linewidth increases with concentration due to the increasing magnetic dipolar interactions between the Eu^{2+} cations, the more dilute phase has a smaller linewidth than the more concentrated phase. The effect of phase separation on the Eu^{2+} EPR spectrum is illustrated at two concentrations within the miscibility gap in Fig. 8. These EPR spectra can be decomposed into narrow and broad components, due to the more dilute and more concentrated phases, respectively. At any point within the miscibility gap derived by visual observation, both the concentrations and relative amounts of the two phases can be estimated and then used as a preliminary check on the EPR data. Using this procedure, we have found that the composite EPR spectra are in good qualitative agreement with the visually observed coexistence curve, both in terms of the relative intensities of the two lines and their linewidths. In the latter case, we found that the two linewidths were nearly equal to those of two solutions prepared at compositions derived from the coexistence curve and held at temperatures just above the phase boundaries. Hence, EPR provides a useful technique to map out the coexistence curve for Eu–NH_3 solutions. In general, we have found that visual observation and EPR determinations of the coexistence curve are in good agreement, with EPR being the more sensitive technique at both low ($\lesssim$0.2 MPM) and high ($\gtrsim$4 MPM) concentrations.

In the metallic region, the EPR lines are highly asymmetric and have the characteristic Dysonian lineshape for slowly diffus-

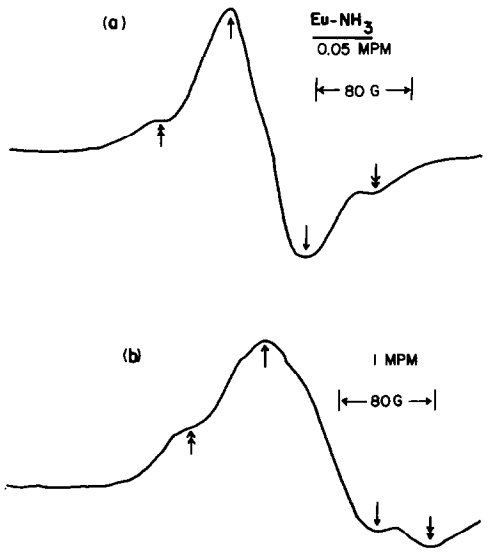

FIG. 8. Typical first-derivative EPR spectra for Eu–NH_3 solutions within the miscibility gap at 255 K and 9.40 GHz. Phase separation is evident in spectra (a) and (b), and the lines due to the more dilute and concentrated phases are indicated by single and double arrows, respectively.

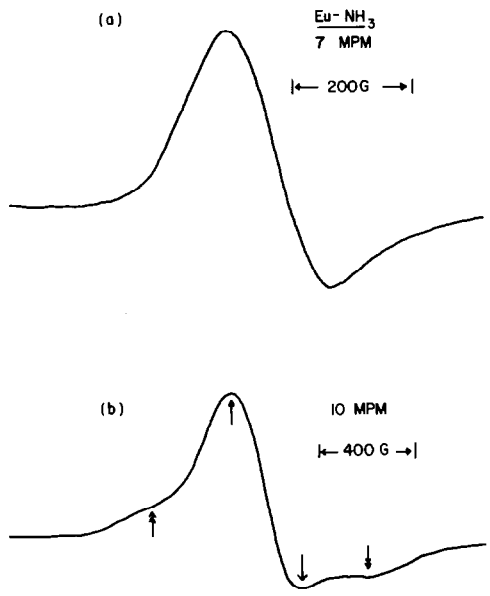

FIG. 9. Typical first-derivative EPR spectra for concentrated Eu–NH_3 solutions at 255 K and 9.50 GHz. Only one phase appears in spectrum (a), whereas two phases are evident in spectrum (b). Single and double arrows identify the lines due to the more dilute and concentrated phases, respectively.

ing magnetic moments (experimental asymmetry parameter $\simeq$ 2–2.5 above about 6 MPM). As shown in Fig. 9, at 255 K only one phase can be detected at 7 MPM, whereas two phases appear at 10 MPM. Although we have not made a detailed study of the phase behavior in the metallic region, reference to the phase diagram of Ca–NH_3 solutions in this same region (Fig. 6), which probably closely resembles the Eu–NH_3 diagram, suggests that at 255 K only one phase is present, whereas there are two phases that may exist at 10 MPM. However, since the width of the narrow line ($\simeq$300 G) is nearly equal to that in solid $Eu(NH_3)_6$ (*24*), the very broad component (width $\simeq$ 900 G) must originate from a new phase having a much higher Eu content, or possibly from Eu or $Eu(NH_2)_2$, which have linewidths of 1300 (*28*) and 1000 G (*26*), respectively.

Discussion

The thermodynamic behavior of different systems near their critical points, such as phase separation in a binary liquid, liquid–vapor condensation, magnetic ordering, etc., is remarkably similar and is best described in terms of critical exponents and order parameters (*29*). The critical-exponent approach has the advantage of universality resulting from the very long-range fluctuations that occur near the critical point, which obviates the need to consider the details of short-range interactions. The order parameter measures numerically the degree and type of ordering near the critical point, and its choice is dictated by the nature of the transition. For instance, the order parameters for phase separation, liquid–vapor condensation, and magnetic ordering are concentration, density, and magnetization, respectively. Using this approach, the general shape of the coexistence curve describing phase separation in M–NH_3 solutions near the critical point can be written (*30*)

$$(x_1 - x_2)/2x_c = [(T_c - T)/T_c]^{\beta}, \qquad (1)$$

where β is the critical exponent and x_1 and x_2 are the mole fractions of M in NH_3 in the more concentrated and more dilute phases, respectively. Theoretically, we expect $\beta = \frac{1}{2}$ if the molecular-field, van der Waals, or Landau theories are valid, in which case the intermolecular forces have an infinite range, and $\beta = \frac{1}{8}$ and 0.313 for the quantum-mechanical two- and three-dimensional Ising models, respectively (*29*). The underlying difference between the Landau and Ising theories is the existence of fluctuations, which are neglected in the former. The Landau theory applies rigorously if the interaction range is infinite, because in this case fluctuations cannot occur. Experimentally, the Landau theory should provide a good description of critical behavior if the interactions have a sufficient range. Con-

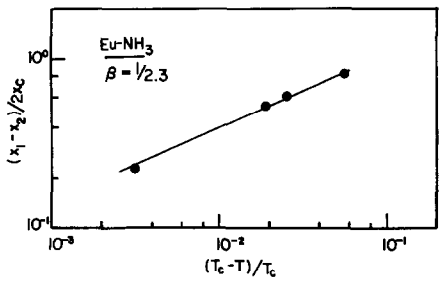

FIG. 10. Logarithmic plot of $(x_1 - x_2)/2x_c$ vs $(T_c - T)/T_c$ for the coexistence curve of Eu–NH_3 solutions. For $(T_c - T)/T_c \lesssim 10^{-1}$, the critical exponent β is 1/2.3.

sistent with this expectation, the Landau theory has been predicted to apply when $(T_c - T)/T_c \gg Z^{-1}$, where Z is the number of interacting neighbors (*31*). Therefore, the Landau theory could be obeyed quite close to T_c if the cluster size is sufficiently large, with a crossover to Ising behavior very close to T_c.

In order to compare theory and experiment, a logarithmic plot of $(x_1 - x_2)/2x_c$ vs $(T_c - T)/T_c$ for Eu–NH_3 solutions is shown in Fig. 10. For $(T_c - T)/T_c$ in the range 3×10^{-3} to 6×10^{-2} MPM, we find $\beta = 1/2.3$, which is fairly close to the value predicted using Landau's theory. Assuming that the Landau theory is valid as long as $Z \gg T_c/(T_c - T)$, we estimate $Z \gg 330$, so that cluster sizes are probably of the order of a few thousand atoms.

Values of the critical exponent β for Li–, Na–, K–, and Ca–NH_3 solutions are also close to $\frac{1}{2}$. Table II summarizes the available values of β for M–NH_3 solutions, the lowest measured reduced temperatures $[(T_c - T)/T_c]_{min}$, for which $\beta \simeq \frac{1}{2}$, and the corresponding lower limit to the cluster size, Z_{min}, near the critical point in the Landau region. It appears that the Landau theory is obeyed approximately for $(T_c - T)/T_c \gtrsim 2 \times 10^{-3}$ and that the cluster sizes near the critical point are quite large. Teoh *et al.* (*12*) have suggested that electronic screening of the cation–electron and electron–electron interactions by the mobile electrons in M–NH_3 solutions provides the mechanism for the apparent long-range interactions in these solutions. Presumably, the three-dimensional Ising theory is obeyed and $\beta = \frac{1}{3}$ very close to T_c. Indeed, there is a suggestion of a crossover to $\beta = \frac{1}{3}$ in Na–NH_3 solutions for $(T_c - T)/T_c \lesssim 2 \times 10^{-3}$ (*8*). Thompson (*32*) has pointed out that β may need to be renormalized due to the presence of mobile electrons, which can be considered to be a hidden variable present at relatively high concentration in conductors. Such hidden variables can result in a higher value of β above a certain reduced temperature $(T_c - T)/T_c$, which depends on the mobile-electron concentration. This possibility is supported by the observation of β close to $\frac{1}{2}$ in conductors if $(T_c - T)/T_c \gtrsim 10^{-2}$, whereas β is close to $\frac{1}{3}$ in nonconductors (*32*). Hence, we expect the reduced temperature at crossover to depend on the electron concentration, which is nearly the same in all M–NH_3 solutions that undergo phase separation (see Table I), so that their crossover reduced temperatures should be nearly the same.

The above critical-exponent approach emphasizes the similarities in diverse systems near their critical points. However, it is clear from Table I that there are some important differences between M–NH_3 so-

TABLE II

CRITICAL PARAMETERS OF METAL–AMMONIA SOLUTIONS

Solution	β^a	$[(T_c - T)/T_c]_{min}$	Z_{min}
Li–NH_3	1/2.2	2×10^{-3}	500
Na–NH_3	1/1.99	2×10^{-3}	500
K–NH_3	1/2.3	3×10^{-3}	330
Ca–NH_3	1/2.2	2×10^{-2}	50
Eu–NH_3	1/2.3	3×10^{-3}	330

[a] Values for Li–, Na–, K–, Ca–, and Eu–NH_3 solutions are derived from Refs. (*16*), (*8*), (*16*), (*12*), and this work, respectively.

lutions, especially between the monovalent and divalent metals. For monovalent *M*–NH_3 solutions, x_c and T_c are approximately equal in Li–, Na–, and K–NH_3 solutions, presumably due to their chemical similarity, and their average values are 4.2 and 215 K, respectively. Sienko (*14*) first pointed out that the valence-electron concentration in these solutions at 4 MPM is very close to that calculated using the Mott criterion for a nonmetal–metal transition:

$$n \gtrsim (0.25/a_H)^3, \qquad (3)$$

where n is the valence–electron density, $a_H = \varepsilon h^2/4\pi^2 m^* e^2$ is the Bohr radius of the electron, ε is the dielectric constant, and m^* is the effective mass of the electron. Since phase separation does not occur in Rb and Cs–NH_3 solutions due to the large size of the cations, it appears that T_c decreases with increasing ionic size, which also occurs in going from Na to K–NH_3 solutions (see Table I). The origin of the anomalously low T_c in Li–NH_3 solutions is unclear, but it may be related to the relatively strong attractive forces between Li and NH_3 (*33*), which leads to the unique compound, $Li(NH_3)_4$, among the alkali metals.

The situation in divalent *M*–NH_3 solutions is more complex. The valence–electron concentrations of the Ca–NH_3 and Eu–NH_3 solutions at x_c are lower and their T_c's much higher than those of the alkali *M*–NH_3 solutions. The lower values of x_c seem surprising at first, since one anticipates that the electron–cation Coulomb attraction should be greater for the divalent metals, which should result in a higher x_c values than for the monovalent metals. However, according to Eq. (2), the lower x_c values for the divalent metals could result from a larger a_H, which implies that ε/m^* is larger than for the monovalent metals. Since ε should be slightly smaller for divalent *M*–NH_3 solutions due to the decreased orientational polarizability of NH_3, the larger ε/m^* probably results from a smaller m^*. If we assume that ε is a constant, then the lower values of x_c for divalent metals can be accounted for if $m^* \simeq 0.9$ m, where m is the electron mass. It is not unreasonable that such "light" electrons exist in divalent *M*–NH_3 solutions, since, using solid-state terminology, their metallic properties originate from the spillover of electrons into the second Brillouin zone or band overlap, in which case the electrons lie near band edges where m^* generally differs from m. Also, in contrast to alkali *M*–NH_3 solutions, in Ca and Eu–NH_3 solutions x_c decreases and T_c increases with ionic size ($r_{Ca^{2+}} = 0.99$ Å and $r_{Eu^{2+}} = 1.12$ Å). The origin of this behavior is unclear, and its general validity must await the determination of the coexistence curves of the other divalent *M*–NH_3 solutions.

In addition to confirming the phase separation observed visually in *M*–NH_3 solutions, the EPR spectra provide information on cation–electron and electron–electron interactions in *M*–NH_3 solutions and are in qualitative agreement with previous work in the one-liquid region (*25, 34*). In particular, the observation of the EPR spectra of solvated electrons, both solvated electrons and Eu^{2+}, and Eu^{2+} as the concentration is increased indicates that electron–cation interactions are weak. That there is indeed some cation–electron interaction follows from the broadening of the solvated-electron line with increasing concentration as well as the weak exchange interactions and low estimated magnetic ordering temperature in $Eu(NH_3)_6$ (*24*). This weak cation–electron interaction implies that weakly bound ion pairs, rather than monomers, are formed in the dilute range and that magnetic dipolar interactions make an important contribution to the linewidth. It follows that the cation–electron interaction and ion-pairing should be even weaker in the monovalent alkali *M*–NH_3 solutions. In this case, the electron spin pairing that occurs

in M–NH_3 solutions perhaps involves e_2^{2-}, rather than cation–electron species like e^-–Eu^{2+}–e^-, since it is difficult to envision how such weak ion-pairing could produce a diamagnetic singlet state. These results support the idea that the valence-electron concentration in M–NH_3 solutions is the primary factor in determining the nature of the nonmetal–metal transition. Complete details of our EPR investigation of Eu–NH_3 solutions will be the subject of a future publication.

Conclusion

The miscibility gap in M–NH_3 solutions provides one of the most striking examples of a nonmetal–metal transition, and the Eu–NH_3 system has the most pronounced miscibility gap among the M–NH_3 solutions that have been investigated. The parabolic shape ($\beta \simeq \frac{1}{2}$) of the coexistence curves in M–NH_3 solutions within close vicinity of their critical points strongly suggests the existence of long-range interactions and concomitant cluster formation.

Several possible mechanisms for the nonmetal–metal transition in M–NH_3 solutions have been discussed by Thompson (*15*), but to date no completely satisfactory theory has been developed. One of the most intriguing questions is whether the driving force for the transition is primarily structural or electronic. In this regard, it is perhaps appropriate to compare the situation in M–NH_3 solutions to that in solids exhibiting a nonmetal–metal transition, which is normally accompanied by a structural distortion. VO_2 is a particularly interesting example, because there is a substantial electronic component to the transition (*6*). In VO_2, the distortion to a lower-symmetry nonmetallic phase containing V–V pairs apparently occurs in an attempt to avoid the formation of the metallic state, in which such pairing is absent. Here the increase in entropy on formation of the metal is overcome by the decrease in electronic energy accompanying partial localization. The same considerations may well apply to M–NH_3 solutions, where an analogous clustering of metal atoms may occur to prevent the formation of the metallic phase.

Both qualitative determinations of the coexistence curves for Sr, Ba, and Yb–NH_3 solutions as well as very precise measurements for one M–NH_3 solution very near T_c are needed if any further progress is to be made in our understanding of the critical behavior of M–NH_3 solutions. Na–NH_3 solutions are the best candidates for detailed study, because the miscibility gap is most pronounced among the alkali metals, the solutions are quite stable near T_c, and precise data already exists down to reduced temperatures of about 10^{-2}. We feel that neutron diffraction represents the best technique to make a precise determination of the coexistence curves of M–NH_3 solutions, since large samples can be used to minimize decomposition, precise temperature control is possible, and the actual distribution of the nonmetallic and metallic phases will not influence the results. As Mike Sienko would have said, such measurements should definitely be pursued, but in *someone else's* laboratory.

Acknowledgments

We thank Dr. Ted White for valuable technical assistance, and Dr. D. T. Peterson of Ames Laboratory at Iowa State University for providing high-purity Eu metal. We also acknowledge the Center for Solid State Science at Arizona State University for use of the state-of-the-art instrumentation within the Magnetism Facility.

References

1. G. Lepoutre and M. J. Sienko (Eds.), "Solutions Métal-Ammoniac," Colloque Weyl I, Benjamin, New York (1964).

2. J. J. LAGOWSKI AND M. J. SIENKO (Eds.), "Metal-Ammonia Solutions," Colloque Weyl II, Butterworth, London (1970).
3. J. JORTNER AND N. R. KESTNER (Eds.), "Electrons in Fluids: The Nature of Metal–Ammonia Solutions," Springer-Verlag, New York (1973).
4. "Electrons in Fluids—The Nature of Metal–Ammonia Solutions," Colloque Weyl IV, *J. Phys. Chem.* **79,** 2789 (1975).
5. "The Fifth International Conference on Excess Electrons and Metal–Ammonia Solutions," Colloque Weyl V, *J. Phys. Chem. 84,* 1065 (1980).
6. F. PINTCHOVSKI, W. S. GLAUNSINGER, AND A. NAVROTSKY, *J. Phys. Chem. Solids* **39,** 941 (1978).
7. W. S. GLAUNSINGER, *J. Phys. Chem.* **84,** 1163 (1980); W. S. Glaunsinger, R. B. Von Dreele, R. F. Marzke, R. C. Hanson, P. Chieux, P. Damay, and R. Catterall, *J. Phys. Chem.,* in press.
8. J. J. LAGOWSKI AND M. J. SIENKO (Eds.), "Metal-Ammonia Solutions," Colloque Weyl II, p. 339, Butterworth, London (1970).
9. J. A. KRUMHANSL, *in* "Physics of High Pressures" (C. T. Tomizuka and R. M. Emrick, Eds.), Academic Press, New York (1965).
10. K. S. PITZER, *J. Amer. Chem. Soc.* **80,** 5046 (1958).
11. N. F. MOTT, *Philos. Mag.* **6,** 287 (1961).
12. H. TEOH, P. R. ANTONIEWICZ, AND J. C. THOMPSON, *J. Phys. Chem.* **75,** 399 (1971).
13. B. WIDOM, *J. Chem. Phys.* **37,** 2703 (1962).
14. G. LEPOUTRE AND M. J. SIENKO (Eds.), "Solutions Metal-Ammoniae," Colloque Weyl I, p. 23, Benjamin, New York (1964).
15. J. C. THOMPSON, "Electrons in Liquid Ammonia," Chap. 4, Oxford Univ. Press (Clarendon), London/New York (1976).
16. P. D. SCHETTLER AND A. PATTERSON, *J. Phys. Chem.* **68,** 2865 (1964).
17. H. K. SCHÜRMANN AND R. D. PARKS, *Phys. Rev. Lett.* **26,** 835.
18. J. W. HODGINS, *Canad. J. Res. Sect. B* **27,** 861 (1949).
19. P. R. MARSHALL AND H. HUNT, *J. Chem. Eng. Data* **7,** 399 (1962).
20. R. L. SCHROEDER, J. C. THOMPSON, AND P. L. OERTEL, *Phys. Rev.* **178,** 298 (1969).
21. R. HAGEDORN AND J. P. LELIEUR, *J. Phys. Chem.* **85,** 275 (1981).
22. J. C. THOMPSON, "Electrons in Liquid Ammonia," Chap. 4, p. 231, Oxford Univ. Press (Clarendon), London/New York (1976).
23. M. J. MOBLEY, W. S. GLAUNSINGER, AND J. C. THOMPSON, *J. Phys. Chem.* **84,** 1168 (1980).
24. F. Y. ROBB, T. R. WHITE, AND W. S. GLAUNSINGER, *J. Magn. Reson.* **48,** 382 (1982).
25. R. CATTERALL AND M. C. R. SYMONS, *J. Chem. Soc.* 3763 (1965).
26. G. F. KOKOSZKA AND N. J. MAMMANO, *J. Solid State Chem.* **1,** 227 (1970).
27. C. A. HUTCHISON AND R. C. PASTOR, *J. Chem. Phys.* **21,** 1959 (1953).
28. M. PETER AND B. T. MATTHIAS, *Phys. Rev. Lett.* **4,** 449 (1960).
29. L. P. KADANOFF, W. GÖTZE, D. HAMBLEN, R. HECHT, E. A. S. LEWIS, V. V. PALCIAUSKAS, M. RAYL, J. SWIFT, D. ASPINES, AND J. KANE, *Rev. Mod. Phys.* **39,** 395 (1967).
30. H. E. STANLEY, "Introduction to Phase Transitions and Critical Phenomena," Oxford Univ. Press (Clarendon), London/New York (1971).
31. R. BROUT, "Phase Transitions," Benjamin, New York (1965).
32. J. C. THOMPSON, "Electrons in Liquid Ammonia," Chap. 4, p. 214, Oxford Univ. Press (Clarendon), London/New York (1976).
33. W. S. GLAUNSINGER AND R. CATTERALL, *J. Phys. Chem.,* in press.
34. D. S. THOMPSON, E. E. HAZEN, AND J. S. WAUGH, *J. Chem. Phys.* **44,** 2954 (1965).